

https://doi.org/10.1070/QEL17113

Laser and thermooptical characteristics of a laser head based on a thin Yb:YAG slab

A.V. Starobor, I.I. Kuznetsov, I.B. Mukhin, O.V. Palashov

Abstract. **Amplification and thermally induced phase distortions in a cw pumped laser head with an active element in the form of a thin Yb:YAG slab are experimentally studied. Lasing characteristics of an emitter based on this laser head are examined. Laser radiation is obtained with an average power of 32 W and a slope efficiency with respect to the absorbed pump power $\eta = 68\%$.**

Keywords: *slab active element, Yb:YAG, thermal effects, thermal lens, high average power.*

1. Introduction

Solid-state diode-pumped lasers based on Yb:YAG slabs are rather promising for application in various technologies. Compact high-power lasers are required in many fields of science and engineering. Among most widely used laser heads with average powers of tens and hundreds of watts, we should point out several extensively developed laser head types differing by the geometry of the active elements (AEs), which can have the form of thin rods, thin discs, and thin slabs.

At present, laser heads based on thin Yb:YAG rods with a simple double-pass optical scheme can operate with gains exceeding 100 [1] and a pulse energy of up to 2.5 mJ [2, 3]. However, further scaling of gain and pulse energy of thin-rod amplifiers is limited by the breakdown threshold. The thin-disk geometry is easily scalable and most appropriate for generation of short pulses. At the same time, the low pump absorption coefficients and low gains make it necessary to design rather complex multipass schemes [4, 5]. Today, the kilowatt level of the average output power is achieved for single-disk lasers with near-diffraction-limited beam quality [4, 5].

Active elements in the form of a thin slab, as well thin-rod AEs, are intermediate between fibre and traditional solid-state AEs. Thin slabs are characterised by a high ratio of the cooled area to the AE volume and, at a thickness below 1 mm, by an almost one-dimensional temperature gradient, which decreases parasitic thermal effects [6, 7]. In contrast to thin-rod AEs [8], slab AEs allow scaling by increasing their transverse dimensions, which makes it possible to achieve a considerably higher power [9].

On the one hand, thin slabs allow one to achieve a high gain and, hence, to develop simple optical schemes of amplifiers; on the other hand, they allow scaling of sizes. Owing to a large active medium volume and a cooling scheme that considerably decreases thermally induced effects, such as thermal lens [10, 11], thin-slab AEs provide the possibility of achieving high output powers. To date, a number of laser schemes with slab AEs and different types of cooling, pumping, and laser beam propagation have been developed. Slab AEs can be pumped in both longitudinal [12–14] and transverse [15–17] directions, including pumping with the use of zigzag rereflections from the AE boundaries [17, 18]. Cooling is mainly fulfilled due to mounting the slab AE on a cooled copper plate by soldering [19, 20] or by using a mechanical contact [12, 21].

We proposed to use AEs in the form of a sandwich structure based on thin Yb:YAG plates with silicon carbide heat sinks directly cooled with water. We used longitudinal pumping by radiation propagating along the AE without rereflections, because this scheme provides the best overlap of the amplified radiation and the pump region. In the present work, we experimentally study amplification and thermally induced phase distortions in a laser head based on the developed AE, as well as the lasing characteristics of the source based on this laser head.

2. Laser head scheme

The active element is a plate made of an YAG crystal doped with Yb ions (2%) with transverse dimensions of 1×6 mm and a length of 11 mm. Silicon carbide (SiC) plates $2.5 \times 6 \times 11$ mm in size serving as heat sinks were glued to the two sides of the AE using an UV-curable polymer adhesive. Pumping and lasing are performed through the optical faces antireflection coated for wavelengths of 969 and 1030 nm. The sandwich structure is directly cooled by a water flow from both sides. The sandwich structure scheme is presented in Fig. 1.

We used pumping by a fibre-coupled diode with a wavelength of 969 nm and the maximum power $P_{\max} = 240$ W. The fibre core diameter was 200 μm; an aspherical collimator with the focal length $f = 3$ cm was placed at the end of the fibre. The diode radiation was directed to the optical surface of the AE using a lens system (*2*) (Fig. 2), which contained either one spherical lens with $f = 10$ cm, which formed a pump beam spot 0.6 mm in diameter; or two cylindrical lenses confocally positioned in the sagittal ($f = 20$ cm) and meridional ($f = 75$ mm) planes, which formed an elliptical pump beam with the principal axes 1.3 and 0.5 mm long; or a combination of a spherical ($f = 20$ cm) and a cylindrical ($f = 20$ cm) lenses, which formed an elliptical pump beam with the principal axes 3.5 and 0.5 mm long. We used single-pass pumping, 68% of which was absorbed for all pump intensity distribution profiles. In contrast to the zigzag geometry [19], the pump and

A.V. Starobor, I.I. Kuznetsov, I.B. Mukhin, O.V. Palashov Institute of Applied Physics, Russian Academy of Sciences, ul. Ulyanova 46, 603950 Nizhny Novgorod, Russia; e-mail: astarobor@mail.ru

Received 26 August 2019; revision received 28 January 2020
Kvantovaya Elektronika **50** (4) 414–418 (2020)
Translated by M.N. Basieva

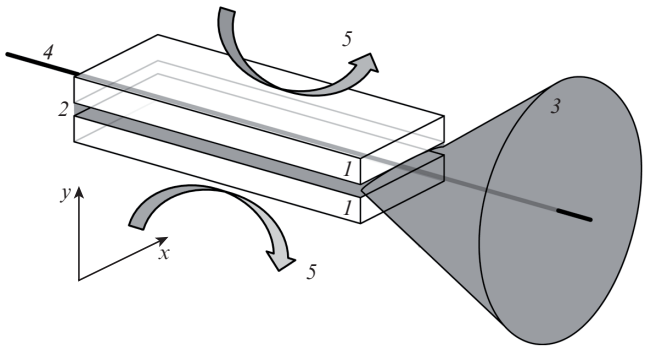

Figure 1. Scheme of the sandwich structure:
(*1*) silicon carbide plates; (*2*) Yb:YAG plate; (*3*) pump diode beam; (*4*) laser beam; (*5*) heat removal directions.

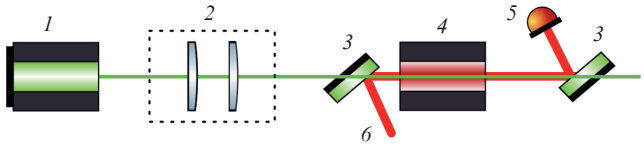

Figure 2. Scheme of pump radiation coupling and gain measurement:
(*1*) pump beam collimator; (*2*) lens system; (*3*) dichroic mirrors; (*4*) laser head; (*5*) photodiode; (*6*) probe beam.

laser beams propagated linearly (like in traditional solid-state AEs) without internal reflections from the lateral surfaces, which provided a good spatial coincidence of these beams [9].

3. Experimental results

Small-signal gain G per pass through the AE in the case of cw pumping with beam spot dimensions of 1.3×0.5 was measured by the probe-beam method (Fig. 2). The probe beam was coupled in through a dichroic mirror (*3*) (Fig. 2), which was transparent at a wavelength of 969 nm and highly reflecting ($R = 99.5\%$) at a wavelength of 1030 nm and placed directly in front of the laser head. The probe beam was modulated with a period of ~20 s by an optomechanical chopper. The beam size exceeded the AE size. A 1-mm diaphragm, which cut off the unamplified part of the probe beam, was placed in front of an FD-24 photodiode (*5*) recording the radiation. We measured the maximum gain corresponding to the maximum population inversion and, hence, to the maximum absorbed pump power density. The diaphragm position was chosen so that the amplified signal was maximum. The gain was measured upon cw pumping after reaching a steady thermal state in the system. This state was reached for a time not exceeding 30 s and was determined by the flow rate and temperature of cooling water. The measured dependence of gain G on the absorbed pump power density is given in Fig. 3.

The maximum gain achieved at the available pump power was $G = 7$. The absence of a bend in the upper part of the curve in Fig. 3 allows us to hope that it is possible to achieve a higher gain by increasing the pump power density.

The thermally induced phase distortions of radiation in the developed laser head were measured using phase-shift interferometry. For this purpose, the laser head was placed in one of the Michelson interferometer arms. The phase incursions in the interferometer shoulder were measured in the presence

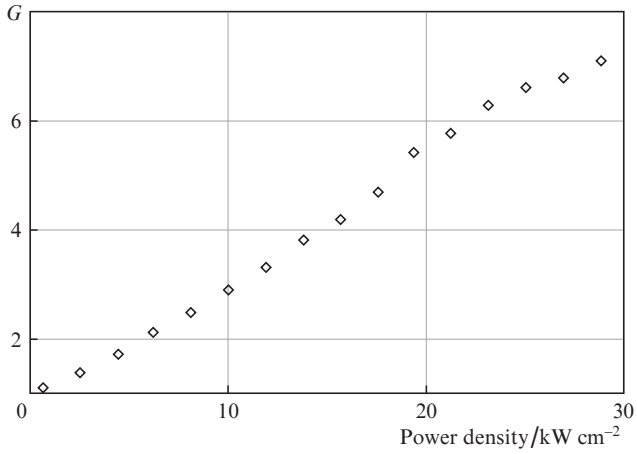

Figure 3. Dependence of the small-signal gain on the absorbed pump power density.

and absence of pumping. The thermally induced phase distortions, i.e., the difference between these two phase incursions, were approximated by a parabola, whose parameters were used to calculate the focal length of the thermal lens.

Figure 4 shows the dependences of the thermal lens power components D_x and D_y appearing along the x and y axes (Fig. 1) on the absorbed pump power for a circular pump spot 0.6 mm in diameter and for an elliptical spot 3.5×0.5 mm in size.

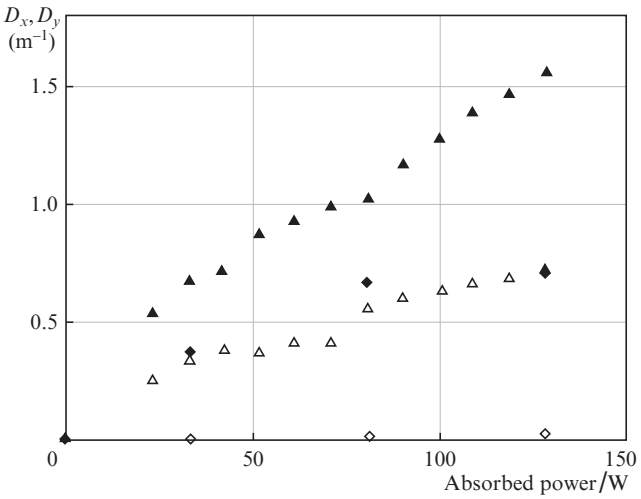

Figure 4. Dependences of the absorbed pump power on the thermal lens optical powers D_x (open symbols) and D_y (filled symbols) for a circular pump spot 0.6 mm in diameter (triangles) and an elliptical spot 3.5×0.5 mm in size (rhombs).

At the circular pump spot, component D_y is considerably (more than twofold) higher than D_x. As the pump spot size increases to 3.5 mm, this difference even increases due to an increase in the transverse temperature gradient, and the thermal lens along the x axis almost disappears.

To verify the obtained data, we constructed a simplified numerical model for calculating the thermal lens for a slab AE. The main, polarisation-independent phase incursion part $\delta(x, y)$ caused by inhomogeneous heating of the AE, can be calculated by the formula [22, 23]

$$\delta(x,y) = \left|\frac{\mathrm{d}n}{\mathrm{d}T}\right|_{\varepsilon=\mathrm{const}} \langle T(x,y,z) - T_0\rangle + \sum_{j=x,y,z} \left|\frac{\mathrm{d}n}{\mathrm{d}\varepsilon_j}\right|_{T=\mathrm{const}} \langle \varepsilon_j(x,y,z)\rangle + (n-1)(1+\nu)\alpha_T \langle T(x,y,z) - T_0\rangle + \mathrm{const}, \quad (1)$$

where n is the refractive index, ε is the deformation, α_T is the temperature expansion coefficient, ν is the Poisson coefficient, and the angular brackets indicate integration over the element length L:

$$\langle \ldots \rangle = \int_0^L \ldots \mathrm{d}z.$$

In the plane-stress approximation and under the condition that the beam propagation along the crystal length can be described by geometric optics laws, the phase incursion, as was shown in [22, 23], can be represented in the form

$$\delta(x,y) = P\langle T(x,y,z) - T_0\rangle, \quad (2)$$

where P is the thermooptical constant responsible for the thermal lens [23]. The main contribution to the thermal lens in Yb:YAG crystals is made by the temperature dependence of the refractive index. For the thermal lens, we assume that

$$P \approx \frac{\mathrm{d}n}{\mathrm{d}T}. \quad (3)$$

Heating of a sample to temperature $T(x,y,z)$ can be calculated from the Poisson equation

$$\Delta_\perp T + \frac{\partial^2 T}{\partial z^2} = -\frac{q(x,y,z)}{\kappa}, \quad (4)$$

where κ is the thermal conductivity and q is the heat release power density. We assume that the heat release power profile in the transverse direction replicates the pump intensity profile and the heat release power is proportional to the pump power.

Averaging Eqn (4) over z and considering the heat release dependence on the transverse coordinates x and y, we obtain

$$\Delta_\perp \langle T\rangle = -\frac{P_{\mathrm{heat}}(x,y)}{\kappa}, \quad (5)$$

where $P_{\mathrm{heat}}(x,y)$ is the heat release power. Then, we numerically solved the linear Poisson equation (5) with the boundary conditions corresponding to the thermally isolated optical and lateral surfaces of the AE. Heat removal from the surfaces bordering the SiC plate was taken to be ideal with a prescribed temperature over the entire interface. In the calculation, the AE cross section was 1×6 mm and the pump spot had an elliptical shape with dimensions varying from 0.5×0.5 mm to 0.5×6 mm. After this, we calculated the focal power D of the thermal lens formed in the sample. The calculated phase incursions and focal powers D_x and D_y of the thermal lens are shown in Figs 5 and 6. Figure 6 also presents the experimental data determined by the slopes of the measured dependences of the thermal lens powers on the absorbed pump power.

For the circular beam, D_x is approximately 30% lower than D_y, which qualitatively agrees with the experimental res-

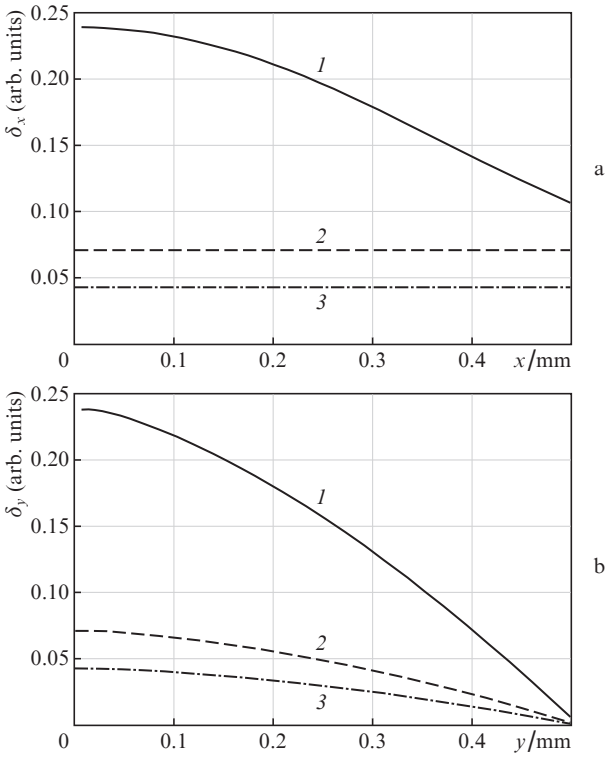

Figure 5. Calculated profiles of thermally induced phases along the (a) x and (b) y axes for beams with identical powers and dimensions of (*1*) 0.5, (*2*) 3.6, and (*3*) 6 mm along the x axis.

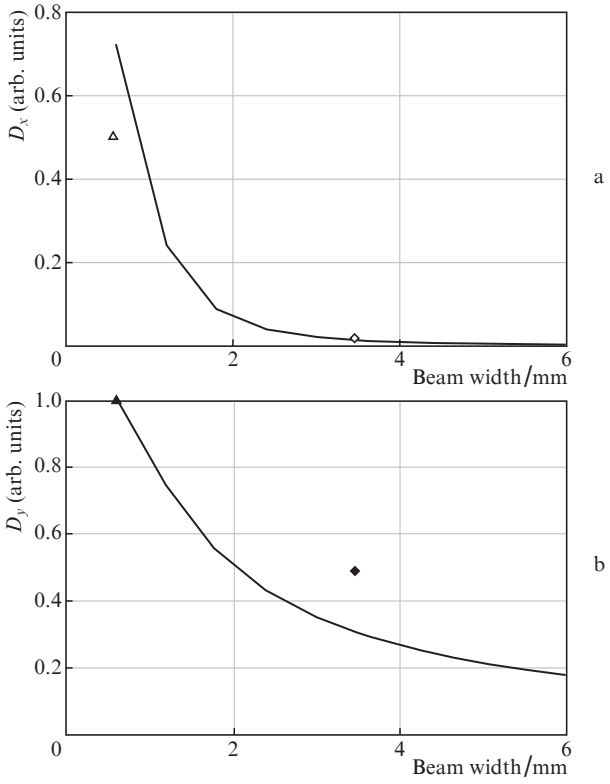

Figure 6. Calculated dependences of the thermal lens powers (a) D_x and (b) D_y on the beam width at identical pump powers. Points indicate the experimental values of D_x and D_y for a circular pump beam with a diameter of 0.6 mm (triangles) and an elliptical beam with dimensions of 3.5×0.5 mm (rhombs).

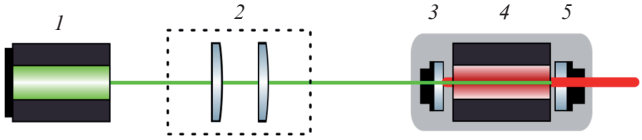

Figure 7. Laser scheme:
(*1*) pump beam collimator; (*2*) lens system; (*3*) dichroic mirror; (*4*) laser head; (*5*) output mirror.

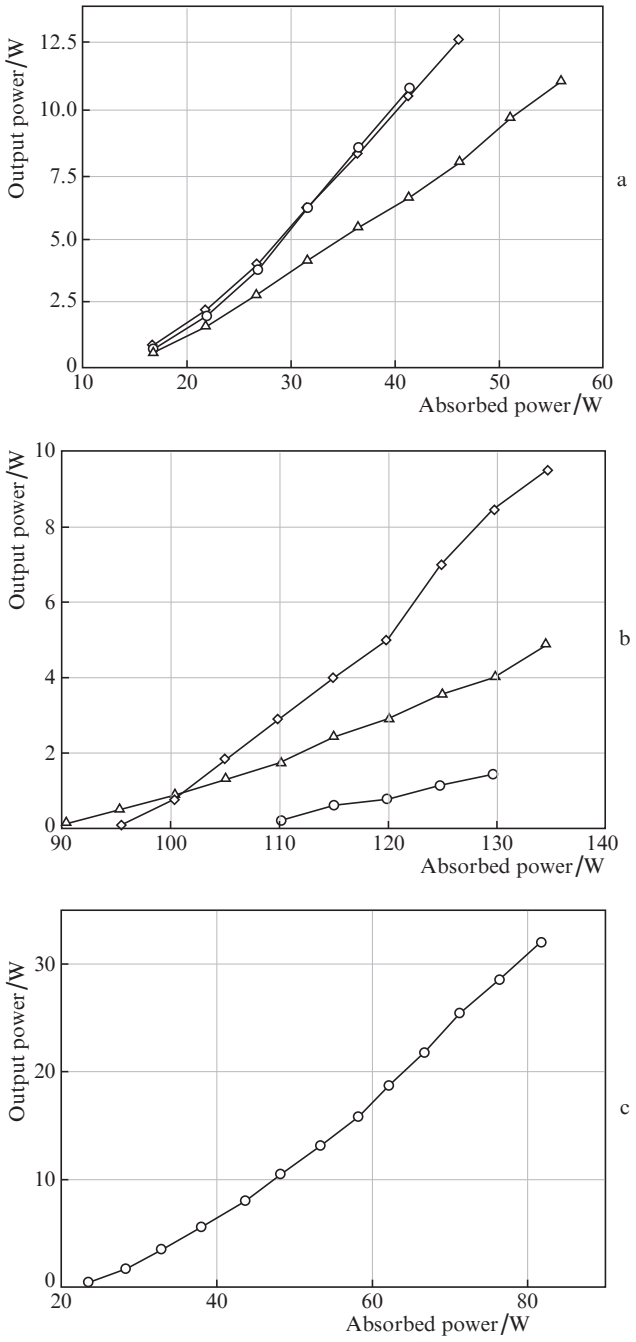

Figure 8. Dependences of the output laser power on the absorbed pump power at output mirror transmittances of 5% (triangles), 10% (rhombs), and 20% (circles) for (a) a circular pump spot 0.6 mm in diameter and (b, c) elliptical spots with dimensions of (b) 3.5 × 0.5 and (c) 1.3 × 0.5 mm.

ults (50% decrease). The focal power D_x decreases by an order of magnitude as the pump spot width increases to 3 mm, while D_y in this case decreases only approximately by three times, which also agrees with the experimental results. Calculations show that the sharp decrease in D_x takes place even when the pump power density does not change with increasing the pump spot width.

The developed laser head was used to develop a highly efficient cw multimode laser. We used a simplest cavity formed by two plane mirrors spaced from each other by 47 mm (Fig. 7).

The dependences of the output laser power on the absorbed pump power are show in Fig. 8 for a circular pump spot 0.6 mm in diameter and an elliptical pump spot with dimensions of 3.5 × 0.5 and 1.3 × 0.5 mm at different transmittances of the output mirror.

The slope efficiency η of the laser was determined as the derivative of the laser power with respect to the absorbed pump power. In the case of a circular pump spot, the slope efficiencies for output mirrors with transmittances of 10 and 20% are almost identical, i.e., η = 45 and 48%, respectively. With increasing the pump spot to an ellipse 3.5 × 0.5 mm in size, the mirror with a transmittance of 10% becomes most efficient, while the slope efficiency in this case decreases to η = 27%.

Figure 9 shows the dependences of the laser power on the absorbed pump power density for different elliptical pump beams and different output mirrors with the optimal transmittance in each case.

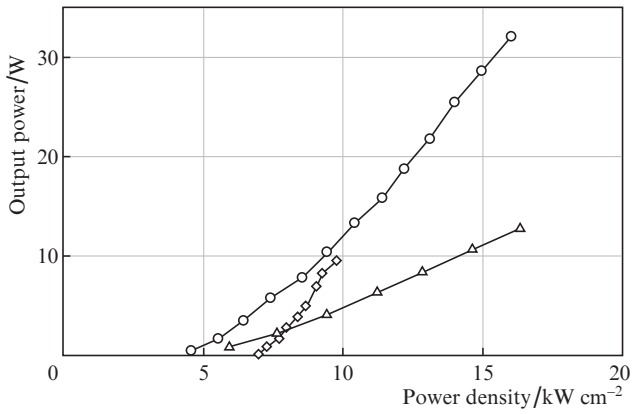

Figure 9. Dependences of the output laser power on the absorbed pump power density at the optimal output mirror transmittance for a circular pump spot 0.6 mm in diameter (triangles) and elliptical spots with dimensions of 3.5 × 0.5 (rhombs) and 1.3 × 0.5 mm (circles).

Analysis of the dependences in Fig. 9 shows that the use of the pump spot with dimensions of 3.5 × 0.5 mm is most efficient with respect to the absorbed pump power, which is most probably related to a lower focal power of the thermal lens.

Pumping with a spot 1.3 × 0.5 mm in size allowed us to achieve an average output power of 32 W at η = 68% and an absorbed pump power of 82 W (Fig. 8c). Today, the output laser power is limited only by the pump power.

4. Conclusions

A laser head based on a thin Yb:YAG slab is developed. The small-signal gain G = 7 is achieved at cw pumping after reach-

ing a steady thermal state in the system. A cw laser with an average output power of 32 W at a slope efficiency $\eta = 68\%$ is developed based on the proposed laser head. Thermally induced phase distortions in the laser head are experimentally studied. It is shown that the thermal lens has a strong astigmatism. Nevertheless, the developed laser head can be successfully used to develop cw and repetitively pulsed lasers with a high average output power and different output radiation parameters.

The high gain and the possibility of scaling the AE dimensions and, therefore, the stored energy, make this laser head especially attractive for application in pulsed laser amplifiers with high-power diode pumping, which operate with high (exceeding 1 kHz) pulse repetition rates and high output powers.

Acknowledgements. This work was supported by the Ministry of Education and Science of the Russian Federation (unique identifier RFMEFI60718X0201).

References

1. Zaouter Y. et al. *Proc. Opt. InfoBase Conf. Pap.* (Baltimore, USA, 2011) pp 3, 4.
2. Délen X. et al. *Opt. Lett.*, **38** (2), 109 (2013).
3. Kuznetsov I. et al. *Opt. Lett.*, **43** (16), 3941 (2018).
4. Nubbemeyer T. et al. *Opt. Lett.*, **42** (7), 1381 (2017).
5. Schad S.-S. et al. *Proc. Conf. Solid State Lasers XXIII: Technol. Devices* (San Francisco, USA, 2014) Vol. 8959, p. 89590U.
6. Eggleston J. et al. *IEEE J. Quantum Electron.*, **20** (3), 289 (1984).
7. Kane T., Eggleston J., Byer R. *IEEE J. Quantum Electron.*, **21** (8), 1195 (1985).
8. Kuznetsov I., Mukhin I., Palashov O. *Proc. 2014 Int. Conf. Laser Optics* (St. Petersburg, Russia, 2014) p. 1.
9. Thomson I.J. et al. *Proc. Conf. Solid State Lasers XIX: Technol. Devices* (San Francisco, USA, 2010) Vol. 7578, p. 75780K.
10. Russbueldt P. et al. *IEEE J. Sel. Top. Quantum Electron.*, **21** (1), 447 (2015).
11. Russbueldt P., Mans T., Rotarius G., Weitenberg J., Hoffmann H.D., Poprawe R. *Opt. Express*, **17**, 12230 (2009).
12. Ganija M. et al. *Opt. Express*, **21** (6), 6973 (2013).
13. Dergachev A. et al. *IEEE J. Sel. Top. Quantum Electron*, **13** (3), 647 (2007).
14. Liu J. et al. *Front. Optoelectron.*, **10** (1), 51 (2017).
15. Liu Q. et al. *J. Opt. Soc. Am. B*, **24** (9), 2081 (2007).
16. Chen Y.-Z.Z. et al. *Chinese Phys. Lett.*, **28** (9), 094208 (2011).
17. Grechin S.G., Nikolaev P.P. *Quantum Electron.*, **39** (1), 1 (2009) [*Kvantovaya Elektron.*, **39** (1), 1 (2009)].
18. Gong M. et al. *Appl. Phys. B*, **79** (3), 265 (2004).
19. Liu F. et al. *Sci. Rep.*, **7** (1), 16699 (2017).
20. Russbueldt P. et al. *Opt. Express*, **17** (15), 12230 (2009).
21. Šulc J. et al. *Proc. Conf. High-Power, High-Energy, High-Intensity Laser Technol. III* (Prague, Czech, 2017) Vol. 10238, p. 1023815.
22. Chénais S. et al. *Prog. Quantum Electron.*, **30** (4), 89 (2006).
23. Mezenov A.V., Soms L.N., Stepanov A.I. *Termooptica tverdotel'nykh lazerov* (Thermal Optics of Solid-State Lasers) (Leningrad: Mashinostroenie, 1986).